Miner Petrol (2017) 111:843–851
DOI 10.1007/s00710-017-0497-z

ORIGINAL PAPER

Batisite, $Na_2BaTi_2(Si_4O_{12})O_2$, from Inagli massif, Aldan, Russia: crystal-structure refinement and high-temperature X-ray diffraction study

Andrey A. Zolotarev Jr[1] · Elena S. Zhitova[1,2] · Faina A. Gabdrakhmanova[1] · Maria G. Krzhizhanovskaya[1] · Anatoly A. Zolotarev[1] · Sergey V. Krivovichev[1,3]

Received: 25 October 2016 / Accepted: 25 January 2017 / Published online: 6 February 2017

Abstract The crystal structure of batisite, $Na_2BaTi_2(Si_4O_{12})O_2$, from the Inagli massif (Aldan, Yakutia, Russia) was refined to R_1 = 0.032 for 1449 unique observed reflections. The mineral is orthorhombic, *Imma*, a = 8.0921(5), b = 10.4751(7), c = 13.9054(9) Å, V = 1178.70(13) Å^3. The mineral is based upon three-dimensional titanosilicate framework consisting of chains of corner-sharing MO_6 octahedra (M = Ti, Nb, Fe and Zr) and *vierer* chains of corner-sharing SiO_4 tetrahedra. Both chains are parallel to the a axis and are linked by sharing peripheral O atoms. The octahedral chains display disorder of M atoms and bridging O sites related to the out-of-center distortion of octahedral geometry around Ti^{4+} cations. Electron microprobe analysis gives SiO_2 39.46, TiO_2 24.66, BaO 21.64, Na_2O 7.56, K_2O 4.38, Fe_2O_3 0.90, ZrO_2 0.66, Nb_2O_5 0.36, $(H_2O)_{calc}$ 0.58, sum 99.76 wt%. The seven strongest X-ray powder-diffraction lines [listed as d in Å (I) *hkl*] are: 8.39 (94) *011*, 3.386 (56) *031*, 3.191 (36) *123*, 2.910 (46) *222*, 2.896 (100) *024*, 2.175 (45) *035*, 1.673 (57) *055*. The thermal behaviour of batisite in the temperature range from 25 to 950 °C was studied using high-temperature powder X-ray diffraction. The thermal expansion coefficients along the principal crystallographic axes are: $\alpha_a = 14.4 \times 10^{-6}$, $\alpha_b = 8.7 \times 10^{-6}$, $\alpha_c = 8.4 \times 10^{-6}$, $\alpha_V = 31.5$ °C^{-1} for the temperature range 25–500 °C and $\alpha_a = 19.6 \times 10^{-6}$, $\alpha_b = 9.1 \times 10^{-6}$, $\alpha_c = 8.8 \times 10^{-6}$, $\alpha_V = 37.6$ °C^{-1} for the temperature range 500–900 °C. The direction of maximal thermal expansion is parallel to the chains of both MO_6 octahedra and SiO_4 tetrahedra, which can be explained by the stretching of silicate chains due to the increasing thermal vibrations of the Ba^{2+} cations. At 1000 °C, the titanosilicate framework in batisite collapses with the formation of fresnoite, $Ba_2TiSi_2O_7O$.

Keywords Batisite · Crystal structure · Thermal expansion · Inagli massif · Fresnoite · Shcherbakovite group

Editorial handling: N. V. Chukanov

Electronic supplementary material The online version of this article (doi:10.1007/s00710-017-0497-z) contains supplementary material, which is available to authorized users.

✉ Andrey A. Zolotarev, Jr
aazolotarev@gmail.com

[1] Institute of Earth Sciences, St. Petersburg State University, St. Petersburg, Russia

[2] Institute of Volcanology and Seismology, Russian Academy of Sciences, Petropavlovsk-Kamchatsky, Russia

[3] Nanomaterials Research Center, Kola Science Center, Russian Academy of Sciences, Apatity, Russia

Introduction

Batisite, $Na_2BaTi_2(Si_4O_{12})O_2$ (Kravchenko et al. 1960), is a chain silicate that is structurally and chemically related to noonkanbahite, $KNaBaTi_2(Si_4O_{12})O_2$ (Uvarova et al. 2010), and shcherbakovite, $K_2NaTi_2(Si_4O_{12})$ O (OH) (Es'kova and Kazakova 1954; Uvarova et al. 2003; Krivovichev et al. 2004). Synthetic analogues of these minerals are of interest due to their nonlinear optical properties (Bloembergen and Pershan 1962; Williams 1984; Gopalakrishnan et al. 1999; Lunkenheimer et al. 2014). In general, Ba titanosilicates display important optical, photoluminescent and afterglow properties that triggered recent research on crystal structure and stability of $BaTiSi_2O_7$ (Viani et al. 2015), which is rather close to the mineral fresnoite $Ba_2TiSi_2O_7O$.

The general formula of the shcherbakovite-group minerals is $A1A2A3M_2\varphi_2[T_4O_{12}]$, where $A1$ = Ba or K; $A2$ = Na or K; $A3$ = Na; M = Ti, Nb, Fe^{3+}, Zr; T = Si; φ = O, OH, F (Uvarova

et al. 2003). Their crystal structures are based upon chains of corner-sharing MO_6 chains and chains of corner-sharing SiO_4 tetrahedra, both running parallel to the *a* axis and linked by sharing peripheral O atoms (Fig. 1). The identity period of the silicate chains contains four tetrahedra with the formula $[Si_4O_{10}]^{8-}$ and therefore can be identified as *vierer* chains according to Liebau (1985) or 'batisite-like chain' according to Nikitin and Belov (1962) and Uvarova et al. (2010). The titanosilicate framework in the crystal structures of shcherbakovite-group minerals is porous and contain three kinds of interstitial voids occupied by the *A*1, *A*2 and *A*3 cations (Fig. 1) (Uvarova et al. 2003; Krivovichev et al. 2004; Uvarova et al. 2010).

Recent crystal-structure studies of the shcherbakovite-group minerals demonstrated that they may adopt both centrosymmetric (*Imma* or *Imcm* in a non-standard setting) (Schmahl and Tillmanns 1987; Uvarova et al. 2003; Krivovichev et al. 2004; Uvarova et al. 2010) and non-centrosymmetric (*Ima*2) (Nikitin and Belov 1962; Rastsvetaeva et al. 1997) space groups (Table 1). The presence (or absence) of inversion center in these structures is determined by the absence (or presence) of polar configurations of

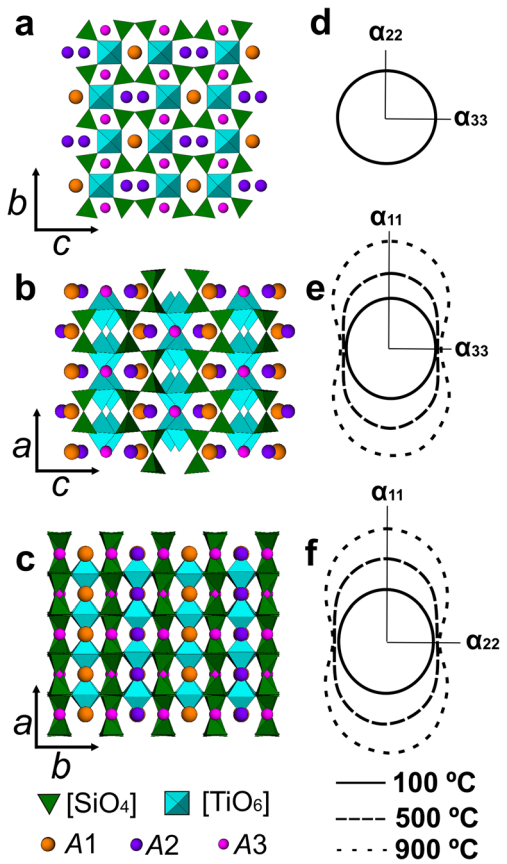

Fig. 1 **a**, **b**, **c** Projections of the crystal structure of batisite along *a*, *b* and *c*, respectively; *d*, *e*, *f* – sections of the figure of thermal expansion coefficients in the respective crystallographic planes. For 011 projection, the figure of thermal expansion coefficients at $T = 100$, 500 and 900 °C coincide

Table 1 Results of the crystal structure refinements of batisite, noonkanbahite and shcherbakovite

Mineral	Batisite	Batisite	Noonkanbahite		Shcherbakovite	Noonkanbahite
Locality	Inagli massif, Russia	Inagli massif, Russia	Eifel, Germany	Eifel, Germany	Khibiny complex, Russia	Eifel, Germany and Murun, Siberia, Russia
Crystal system	Orthorhombic					
Space group	*Imma*	*Ima*2	*Imcm*	*Ima*2	*Imma*	*Imma*	*Imma*
a (Å)	8.0921	10.40	10.499	10.505	8.1538	8.1511	8.0884
b (Å)	10.4751	13.85	13.913	13.895	10.5569	10.5502	10.4970
c (Å)	13.9054	8.10	8.087	8.142	13.9882	13.9784	13.9372
V (Å^3)	1178.70	1166.7	1181.3	1186.5	1204.1	1202.1	1183.3
R_1	0.032	0.174	0.078	0.047	0.032	0.033	0.028
References	this work	Nikitin and Belov (1962)	Schmahl and Tillmanns (1987)	Rastsvetaeva et al. (1997)	Uvarova et al. (2003)	Krivovichev et al. (2004)	Uvarova et al. (2010)

the MO_6 chains that consists of alternating long and short apical *M*-O bond lengths (Krivovichev et al. 2004). In the non-centrosymmetric model, vectors of short *M*-O bonds have the same ordered orientation, whereas in the centrosymmetric model, these vectors have opposite orientations, which results in the observed structural disorder for the *M* sites and the sites of bridging O atoms (Fig. 2). It seems very probable that the minerals may exist in both centrosymmetric and non-centrosymmetric modifications as it was earlier suggested by Rastsvetaeva et al. (1997), depending upon the size of ordered polar domains, by analogy with vesuvianite-group minerals (Allen and Burnham 1992; Armbruster and Gnos 2000). Therefore, symmetry of shcherbakovite-group minerals may well be related to the conditions of their formation in nature (Krivovichev et al. 2004).

Although the structural and crystal chemical features of the minerals of this group have been studied previously, the crystal structure of batisite was refined only in 1962 (Nikitin and Belov (1962)), and the refinement was not of perfect quality (0.174). The purpose of this study is to report on the results of the crystal-structure refinement of batisite and to investigate its thermal behavior by means of the high-temperature powder X-ray diffraction.

Materials and methods

The sample of batisite used in this study was taken from the collections of the Mineralogical Museum of St. Petersburg State University, where it is stored under catalogue number № 2/16977. The sample originates from the Inagli chromium deposit (Inagli massif, Aldan shield, Yakutia, Russia), the holotype locality for the mineral (Kravchenko et al. 1960). However, there is a possibility that the sample studied is not exactly the same sample of batisite that were studied previously by Kravchenko et al. (1960), because of the minor differences in their chemical compositions (Table 2). Batisite was originally found in an aegirine-arfvedonite-microcline pegmatite in dunites (Kravchenko et al. 1960).

The chemical composition of batisite sample 2/16977 was determined by means of Hitachi S-3400 N EPMA (electron probe micro-analyser) equipped with wavelength-dispersive INCA 500 spectrometer. The system was operated at 20 kV and 10 nA and the electron beam was focused to a 5 μm spot. The counting time was 30 s in point. The following calibrant materials were used: quartz (Si), baryte (Ba), albite (Na), goethite (Fe), orthoclase (K), rutile (Ti), zircon (Zr), metallic Nb (Nb). No elements other than those mentioned above were detected. The mean analytical results (average over 6 points) as well as ranges for each oxide component are presented in Table 2.

Single-crystal X-ray diffraction data were collected by means of a Bruker Duo X-ray diffractometer operated at 45 kV and 0.6 mA (microfocus source) and equipped with a CCD detector using monochromatic MoKα X-radiation, frame widths of 0.5° in ω and 10 s counting time for each frame. The unit-cell parameters were refined on the basis of 5115 unique reflections (Table 3). The intensity data were reduced and corrected for Lorentz, polarization and

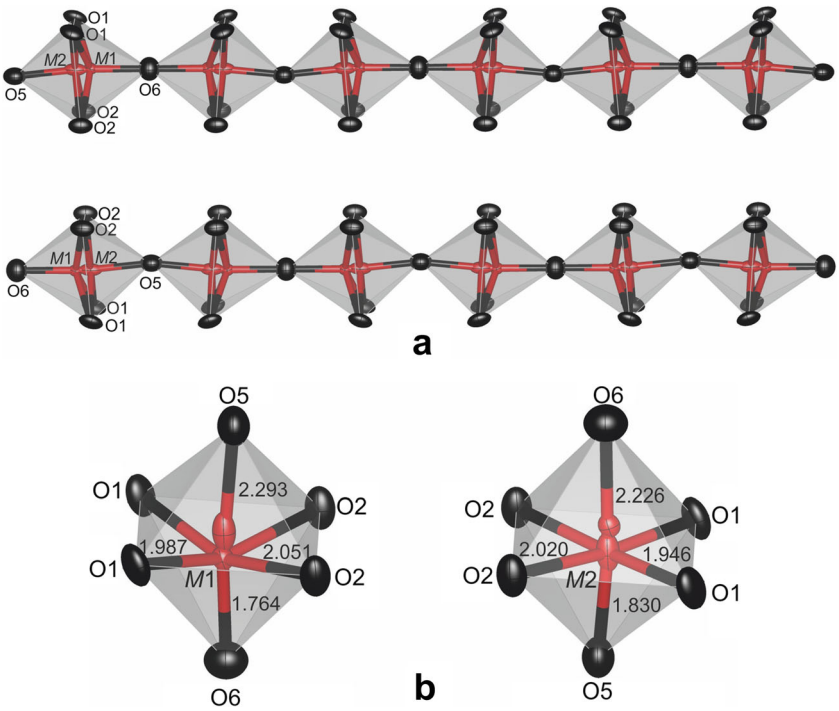

Fig. 2 **a** MO_6 chains in the batisite structure: centrosymmetric model; **b** – coordination of the *M*1 and *M*2 sites with respective bond lengths (in Å). Ellipsoids of thermal vibrations are drawn at the 80% probability 1eve1

Table 2 Chemical composition and chemical formula for batisite

Oxide	wt% Min	wt% Max	wt% Mean	Element	a.p.f.u (calculated on the basis of 4 Si)	Oxide	wt%
this work						from the holotype locality (Kravchenko et al. 1960)	
SiO_2	37.78	42.23	39.46	Si	4.00	SiO_2	39.00
Fe_2O_3	0.84	0.96	0.90	Fe	0.07	Fe_2O_3	1.80
BaO	21.21	22.03	21.64	Ba	0.86	BaO	22.00
Na_2O	7.17	8.11	7.56	Na	1.49	Na_2O	8.40
Nb_2O_5	0.24	0.46	0.36	Nb	0.02	Nb_2O_5	0.36
K_2O	4.30	4.48	4.38	K	0.57	K_2O	2.60
TiO_2	23.63	24.66	24.22	Ti	1.85	TiO_2	22.00
ZrO_2	0.61	0.74	0.66	Zr	0.03	ZrO_2	1.90
H_2O[a]			0.58	H	0.39	H_2O[a]	0.50
Total			99.76	O	13.98	Al_2O_3	0.90
						CaO	0.27
						SrO	0.03
						MnO	0.09
						Total	99.95

[a] calculated value based on the electroneutrality of the formula taking into account that all Fe considered as a trivalent following for previous studies (Kravchenko et al. 1960; Uvarova et al. 2010)

background effects using the Bruker software APEX2 (Bruker-AXS 2014). A semiempirical absorption-correction based upon the intensities of equivalent reflections was applied (SADABS, Sheldrick 2008). The structure was solved and refined with the ShelX program package (Sheldrick 2008) within the Olex2 shell (Dolomanov et al. 2009). Occupancies of the cation sites were calculated from the experimental site-scattering factors, taking into account cation coordination parameters and empirical chemical composition. In total, four crystals of batisite from Inagli massif were studied and crystal-structure refinements for all of them were performed in both centrosymmetric (*Imma*) and non-centrosymmetric (*Ima*2) space groups. However, we have observed no indications for the preference for the non-centrosymmetric model. Crystallographic data, parameters of data collection and refinement are given in Table 3. The final atomic coordinates, isotropic displacement parameters, refined site-scattering values and assigned populations for selected sites are listed in Table 4; anisotropic-displacement parameters are given in supplementary Table S1, and selected interatomic distances are reported in Table 5.

The thermal behaviour of batisite was studied by in situ high-temperature X-ray diffraction (HTXRD) in the 25–1000 °C temperature range in air by a Rigaku Ultima IV powder X-ray diffractometer (CuKα_{1+2} radiation, 40 kV/30 mA, Bragg-Brentano geometry, PSD D-Tex Ultra) equipped with a high-temperature camera. HTXRD pattern is presented in Fig. 3. The temperature step and the heating rate were 50 °C and 5 °/min, respectively. Thin powder sample was deposited on a Pt sample holder (20 × 12 × 2 mm^3) from a heptane suspension. The unit-cell parameters at all temperatures were refined by the Rietveld method using the program package Topas 4.2 (Bruker AXS 2009). Neutral scattering factors were used for all atoms. The background was modeled using Chebychev polynomial approximation 10th order. The peak profile was described using the fundamental parameters approach. The refinement of preferred orientation parameters confirms the presence of preferred orientation along the [101] direction. The unit-cell parameters at different temperatures refined by the Rietveld method are given in supplementary Table S2.

IR spectra were recorded by means of a Bruker Vertex 70 IR spectrometer at room temperature, using the KBr pellets technique. The data were processed using OPUS program (Bruker 2004).

Results

Chemical composition

The results of chemical analyses by means of EPMA analysis (Table 2) confirm that the mineral should be identified as batisite and has the following empirical formula (calculated on the basis of Si = 4): $(Na_{1.49}Ba_{0.86}K_{0.57})_{\sum 2.92}(Ti_{1.85}Fe^{3+}_{0.07}Zr_{0.03}Nb_{0.02})_{\sum 1.97}(Si_4O_{12})(O_{1.61}OH_{0.39})_{\sum 2.00}$. Table 2 also provides the analytical data for batisite from the holotype locality (Kravchenko et al. 1960), which are slightly different from those obtained for our sample in the Ti, Zr, and

Table 3 Crystallographic data and refinement parameters for batisite

Crystal chemical data	
Crystal system	Orthorhombic
Space group	*Imma*
a (Å)	8.0921(5)
b (Å)	10.4751(7)
c (Å)	13.9054(9)
Unit-cell volume (Å^3)	1178.70(13)
Z	4
Calculated density (g/cm^3)	3.431
Absorption coefficient	4.878
Data collection	
Temperature (K)	293(2)
Radiation	Mo-*Kα*,
Wavelengths (Å)	0.71073
θ range (°)	2.43–39.14
h, *k*, *l* ranges	-9 → 14, −18 → 13, −23 → 24
Total reflections collected	6159
Unique reflections (R_{int})	1797 (0.0384)
Unique reflections $F > 2\sigma(F)$	1449
Structure refinement	
Refinement method	Full-matrix least-squares on F^2
Weighting coefficients *a*, *b**	0.0174, 3.8320
Extinction coefficient	0.0080(3)
Data/ restrains/ parameters	1797/0/84
R_1 [$F > 4\sigma(F)$]	0.0315
wR_2 [$F > 4\sigma(F)$]	0.0674
R_1 all,	0.0430
wR_2 all	0.0723
Goodness-of-fit on F^2	1.044
Largest diff. Peak and hole (*e*Å^{-3})	2.16, −2.16

Fe contents (Kravchenko et al. 1960; Uvarova et al. 2010).

Crystal structure

The structure model obtained for batisite is consistent with the results of the previous studies (Nikitin and Belov 1962; Rastsvetaeva et al. 1997; Uvarova et al. 2003; Krivovichev et al. 2004; Uvarova et al. 2010). The octahedral *M* site is split into two sites, *M*1 and *M*2, located from each other at the distance of 0.46 Å. The average < *M*1-O > and <*M*2-O > distances are 1.999 and 2.024 Å, respectively. The MO_6 octahedra are strongly distorted owing to the electronic second-order Jahn-Teller effect (Kunz and Brown 1994): there are one short (1.830/1.764 Å) and one long (2.226/2.292 Å) *M*-O apical bonds and four average (1.95–2.05 Å) equatorial bonds (Table 5). As it was mentioned above, the Na, Ba and K (sites *A*1-*A*3) are located within three different voids of the octahedral-tetrahedral titanosilicate framework (Fig. 1). Occupancy of cation sites are presented in Table 4. We observed that O4 site, which is bridging between two SiO_4 tetrahedra, is also split into two sites, O4 and O4A, located at 0.60 Å from each other.

High-temperature powder X-ray diffraction

The analysis of powder pattern obtained at room temperature revealed single batisite phase. The data were indexed using calculated powder X-ray pattern from reported herein crystal structure. The seven strongest measured X-ray powder-diffraction lines [listed as d in Å (I) *hkl*] are as follows: 8.39 (94) *011*, 3.386 (56) *031*, 3.191 (36) *123*, 2.910 (46) *222*, 2.896 (100) *024*, 2.175 (45) *035*, 1.673 (57) *055*.

The dependences of the unit-cell parameters of batisite upon temperature are plotted in Fig. 4. The equations are second-order polynomials and are as follows:

$$a = 8.0958 + 6.3 \times 10^{-5} \times T + 5.4 \times 10^{-8} \times T^2$$

$$b = 10.465 + 8.5 \times 10^{-5} \times T + 6.0 \times 10^{-9} \times T^2$$

$$c = 13.889 + 1.1 \times 10^{-4} \times T + 7.7 \times 10^{-9} \times T^2$$

$$V = 1176.71 + 27.960 \times 10^{-3} \times T + 9.689 \times 10^{-6} \times T^2$$

The main values of thermal expansion coefficients were determined using second-order approximation of temperature dependencies in the temperature range of 25–950 °C by the TEV program (Langreiter and Kahlenberg 2014). The thermal expansion coefficients along the principal crystallographic axes are listed in supplementary Table S3. The TEV program (Langreiter and Kahlenberg 2014) was also used for the visualization of figure of thermal expansion coefficients (Fig. 1d, e, f).

In order to investigate the influence of temperature upon the crystal structure of batisite, its single crystals were annealed at 800 °C for 4 h. However, structure refinement of the annealed crystals did not show any significant deviations from the crystal-structure data for the crystals before annealing.

IR-spectroscopy

The IR spectrum (4000–300 cm^{-1}) for batisite is shown in Fig. 5. The region of the spectra 1500–300 cm^{-1} is similar to that provided by Chukanov (2014), where the main absorption bands are attributed to symmetric and asymmetric lattice vibrations (e.g. Si-O, Si-O-Si, Ti-O). The region 4000–2000 cm^{-1} of IR spectra was not reported by Chukanov (2014) and other studies. Our study reveals the presence of an intense broad band around 3450 cm^{-1} and a broad shoulder at 3300–2850 cm^{-1}. The slight absorption was also detected

Table 4 Atomic coordinates, site-scattering values, bond valence sums, occupancies and equivalent isotropic displacement parameters U_{eq} (Å^2) for batisite

Atom	s.s. [a]	*x*	*y*	*z*	Site occupancy	calc. s.s.[a]	BVS [b]	U_{eq}
*A*1	50.27	0	0.25	0.25230(2)	$Ba_{0.85}K_{0.15}$	50.45	1.70 [1.95]	0.01155(8)
*A*2	13.76	0	0.25	0.6798(2)	$Na_{0.65}K_{0.35}$	13.80	0.76	0.0296(7)
*A*3	11.00	0	0.5	0.5	Na	11.00	1.06	0.0259(5)
*M*1	12.88	0.225(1)	0.25	0.4690(1)	$Ti_{0.54}Fe_{0.025}$ $Zr_{0.01}Nb_{0.005}$	13.14	2.30	0.0127(8)
*M*2	9.63	0.282(1)	0.25	0.4712(2)	$Ti_{0.39}Fe_{0.01}$ $Zr_{0.01}Nb_{0.01}$	9.65	1.50	0.0067(6)
Si	14.00	0.3037(8)	0.47314(5)	0.64517(4)	Si		4.14	0.0093(1)
O1	8.00	0.2208(2)	0.3827(1)	0.5669(1)	O		2.10	0.0163(3)
O2	8.00	0.2488(2)	0.6204(1)	0.6377(1)	O		1.97	0.0157(3)
O3	8.00	0.25	0.4173(2)	0.75	O		2.14	0.042(1)
O4	4.60	0.5	0.4611(9)	0.663(1)	$O_{0.60}$	4.80	1.24 [1.31]	0.029(3)
O4a	3.52	0.5	0.4696(8)	0.620(2)	$O_{0.40}$	3.20	0.78	0.025(3)
O5	8.00	0	0.25	0.4553(2)	O		1.74	0.0183(6)
O6	8.00	0.5	0.25	0.4699(3)	O		1.34 [1.45]	0.0211(7)

[a] s.s. – site scattering and calc. s.s. – calculated site scattering (e.p.f.u)

[b] BVS – bond valence sums: bond-valence parameters according Brese and O'Keeffe (1991); bond-valence values calculated on the basis of following sites composition: *A*1 = $Ba_{0.85}$ $K_{0.15}$ (for *A*1 CN is 9, values in [ ] calculated for CN = 12); *A*2 = $Na_{0.65}$ $K_{0.35}$; *A*3 = Na; and in view of split positions: *M*1 = $Ti_{0.60}$ and *M*2 = $Ti_{0.40}$; O4 = $O_{0.60}$ and O4A = $O_{0.40}$

around 1650–1600 cm^{-1} (Fig. 5). In general, the IR spectrum shows the presence of OH-groups (absorption below 3300 cm^{-1}) and H_2O molecules (the band at 1600–1650 cm^{-1}). The H_2O molecules are not a part of the crystal structure and probably belong to the admixture of alteration products.

Table 5 Selected interatomic distances in the structure of batisite

*A*1-O5	2.823(3)	*M*1-O5	1.830(9)
*A*1-O2	2.870(2) × 4	*M*1-O1	1.946(2) × 2
*A*1-O2	2.918(2) × 4	*M*1-O2	2.020(2) × 2
*A*1-O6	3.090(4)	*M*1-O6	2.226(9)
*A*1-O4	3.273(6) × 2	<*M*1-O>	1.999
<*A*1-O>	2.968		
		*M*2-O6	1.764(8)
		*M*2-O1 × 2	1.987(3)
*A*2-O1	2.755(2) × 4	*M*2-O2 × 2	2.051(3)
*A*2-O3	2.849(2) × 4	*M*2-O5	2.292(8)
<*A*2-O>	2.801	<*M*2-O>	2.024
		Si-O1	1.591(2)
*A*3-O1	2.360(2) × 4	Si-O2	1.608(2)
*A*3-O5	2.691(1) × 2	Si-O3	1.630(1)
<*A*3-O>	2.470	Si-O4	1.612(4)
		Si-O4A	1.627(5)
		<Si-O>	1.613

Discussion

One of the aims of this study was to determine the most suitable structural model for batisite from the Inagli massif, i.e. the presence or absence of ordered arrangement of polar MO_6 chains and, as a consequence, the presence or absence of an inversion symmetry center. The principal feature of the non-centrosymmetric structural model reported by Rastsvetaeva et al. (1997) is the ordering of polar octahedral chains with axes consisting of alternating short (~ 1.8 Å) and long (~ 2.3 Å) *M*-O bonds. In the centrosymmetric model, the arrangement of the polar chains is disordered and, as a consequence, the symmetry center is absent. Fig. 2 illustrates the average (disordered) model of the MO_6 chains in the centrosymmetric (space group *Imma*) model and the coordination of the *M*1 and *M2* sites. In order to clarify the problem with respect to our sample, crystal-structure refinement was done in centrosymmetric *Imma* and non-centrosymmetric *Ima*2 space groups (both CIFs are deposited as supplemental electronic material). The crystallographic agreement indices for both groups were approximately the same, but the refinement in the space group *Ima*2 led to the larger values of standard errors of the bond lengths and displacement parameters of the atoms. The values of the Flack (x) and Hooft (y) parameters for the non-centrosymmetric group *Ima*2 were quite high, 0.41(6) and 0.40(6), respectively. Introduction of the racemic twinning improved the quality of refinement only slightly, but the Hooft (y) parameter was still high 0.46(4). In addition, verification of the *Ima*2 cif-file via specialized program

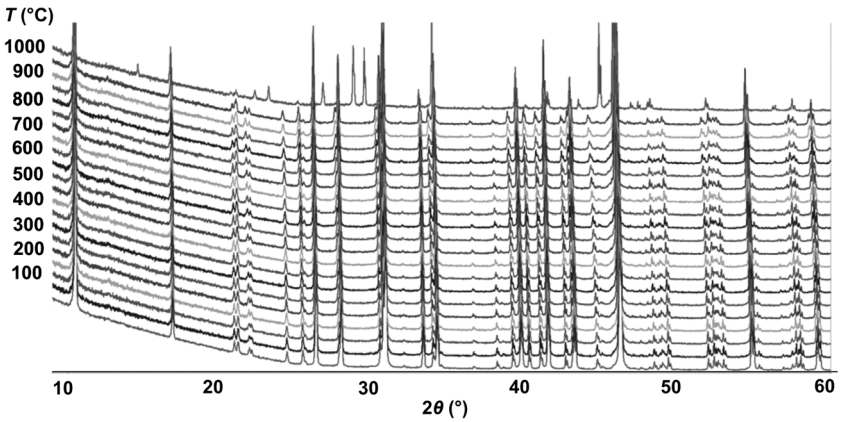

Fig. 3 The evolution of X-ray diffraction (HTXRD) powder patterns of batisite with temperature. In the 25–950 °C temperature range, only batisite is present. At 1000 °C batisite decomposes with the formation of fresnoite

PLATON/ADDSYM (Spek 2009) and website http://checkcif.iucr.org invariably demonstrated the presence of an inversion center. However, the major observation in support of the centrosymmetric model was that the splitting of the octahedral site *M* was observed for both space groups, which is indication that it is not an artifact of the crystal-structure refinement in the centrosymmetric group but the intrinsic property of the structure. It is noteworthy that the same observation was also valid for shcherbakovite (Krivovichev et al. 2004). As it was mentioned above, the single-crystal X-ray diffraction study did not reveal any particular differences relative to the previous studies, except for the more precise values of geometrical parameters (bond lengths and angles) and the splitting of the O4 site, which deserves more attention. The O4 atom is bridging between two adjacent Si atoms with the almost linear Si-O-Si arrangement (the Si-O4-Si angle of 174° (Schmahl and Tillmanns 1987)). We believe therefore that the splitting of the O4 site is not related to the splitting of the *M* position and can be explained by the deviation of Si-O-Si angle from the straight arrangement (Si-O4-Si = 160°, Si-O4A-Si = 155°).

The problem of the role of the OH-groups in the batisite-group minerals was discussed in detail for noonkanbahite (Uvarova et al. 2010) and shcherbakovite (Uvarova et al. 2003). We note that, for noonkanbahite, the presence of OH groups was confirmed by the chemical and SIMS analyses (Uvarova et al. 2010). In our sample, the location and the amount of the OH groups is very similar to those observed in noonkanbahite and shcherbakovite. The presence of hydroxyl groups is confirmed by the absorption band and shoulders around 3600–2850 cm^{-1} in the IR spectrum (Fig. 5). The amount of the OH groups in batisite was calculated on the basis of electroneutrality of the formula. By analogy with noonkanbahite and shcherbakovite, calculation of the bond-valence sums for batisite shows under-saturation of the O6 site (1.34 [or 1.45] v.u. (valence unit), see Table 4), which indicates that this site is partially occupied by hydroxyl groups.

Uvarova et al. (2003) suggested that, in shcherbakovite, the splitting of the *M* site is associated with the incorporation of OH groups into the O6 site (and perhaps the O5 site as well). The ratio *M1*:*M2* of the splitted sites is controlled by the amount of O and OH in the O6 site: in the case of shcherbakovite, the O^{2-} :$(OH)^-$ ratio is approximately 1:1, which correlates well with the equal occupancies of the splitted *M1* and *M2* sites (Uvarova et al. 2003). In our case, the ratio of *M1*:*M2* is around 0.60:0.40 (Table 4), whereas the O^{2-} :$(OH)^-$ is also approximately 0.60:0.40 (according to the chemical data), in good agreement with the model suggested by Uvarova et al. (2003).

For the cation sites, the site-scattering factors (calculated taking into account the chemical composition data) and the bond valence sums are in good agreement as well (Table 4).

As it can be seen from the data listed in supplementary Table S3, the thermal expansion of batisite within the *bc* plane is nearly isotropic (Fig. 1d), whereas the expansion along the *a* axis is significantly stronger. Moreover, the anisotropy becomes even more prononuced in the range of 500–900 °C, when the α_a coefficient increased (α_a = 19.6 $°C^{-1}$) in comparison to those observed for the temperature ranges 25–100 °C and 100–500 °C (14.4 and 8.0 $°C^{-1}$, respectively (Table S3)). The anisotropic thermal expansion of batisite can be explained by the anisotropic distribution of bond strength within its titanosilicate framework. The weakest cation-anion bonds in the framework are long *M*-O bonds induced by the out-of-center distortion of the MO_6 octahedra, owing to the electronic second-order Jahn-Teller effect (Kunz and Brown 1994). These long *M*-O bonds are oriented approximately parallel to [100], which explains the observed thermal-expansion anisotropy. The expansion along the *a* axis is also accompanied by the stretching of the $[Si_4O_{10}]$ chains, which agrees well with their flexibility (Belov 1961; Liebau 1985). Moreover, it has been observed that temperature-induced vibrations of Ba^{2+} cations induce stretching of silicate chains, being responsible for the unusual thermal expansion behaviour of Ba silicates (Liebau 1982; Gorelova et al. 2016; Shapenkov et al. 2017).

At 1000 °C, batisite decomposes with the formation of fresnoite, $Ba_2TiSi_2O_7O$ (Fig. 3). The crystal structure of the latter (Moore and Louisnathan 1969) consists of alternating

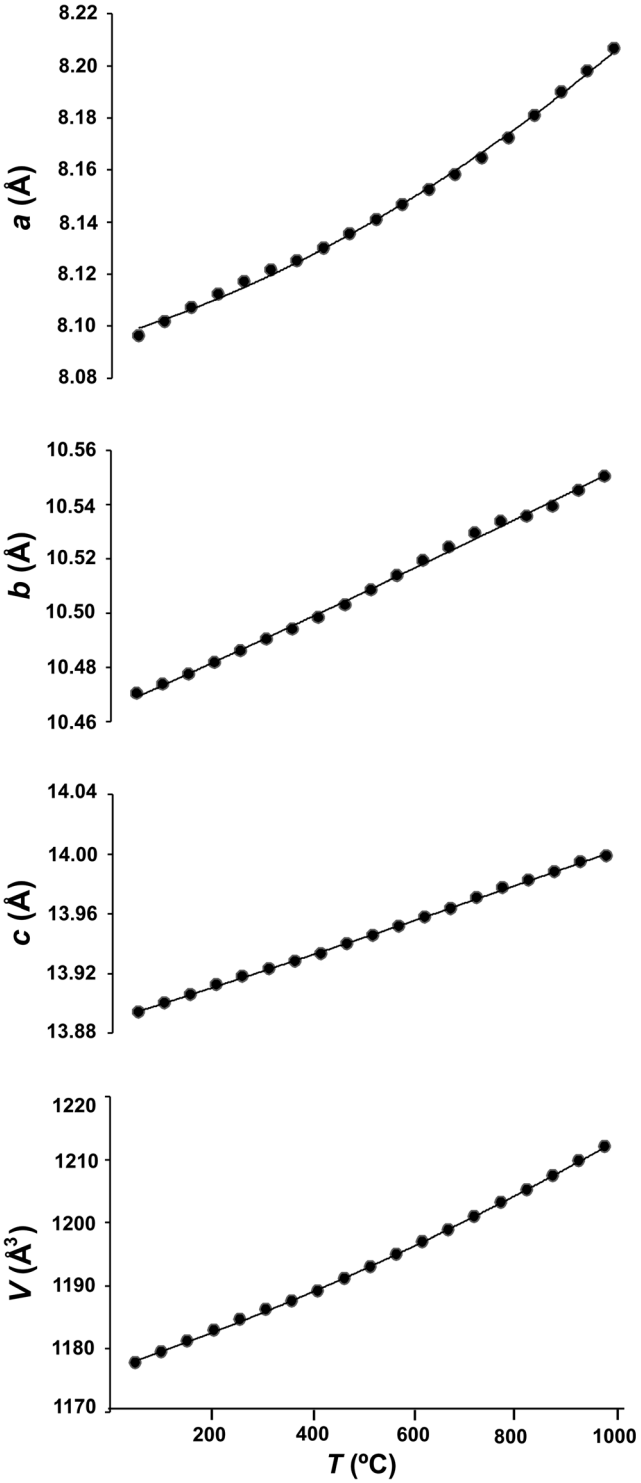

Fig. 4 The evolution of unit-cell parameters of batisite upon heating in the 25–950 °C temperature range (ESDs fall within limits of the symbols)

layers of Ba^{2+} cations and heteropolyhedral sheets formed by TiO_5 square pyramids sharing equatorial corners with Si_2O_7 groups (*T*) (Fig. 6).

It is of interest that the structure of fresnoite has many similarities to that of batisite and can be produced from the

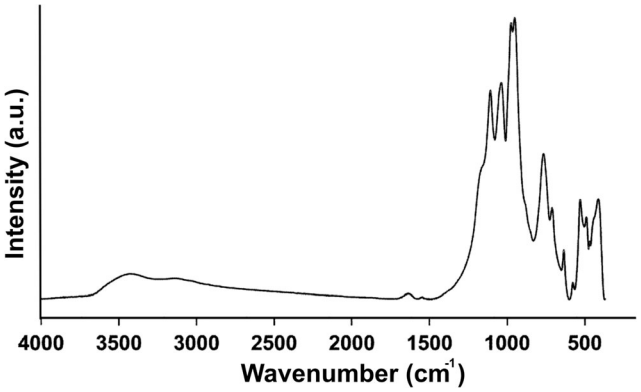

Fig. 5 IR spectrum of batisite

latter by the following series of transformations: (i) chains of corner-sharing TiO_6 octahedra are split into the columns of isolated TiO_5 pyramids; (ii) chains of corner-sharing SiO_4 tetrahedra are split into isolated Si_2O_7 groups (Fig. 6b); (iii) Ti-polyhedra and Si-tetrahedra re-arrange within the *bc* plane for batisite (the *ab* plane for fresnoite) to form five-membered rings.

Due to the high melting point, fresnoite is often considered as a result of high-temperature crystallization as one of the first crystalline products of magmatic fluid contacting with host rocks (Moore and Louisnathan 1969). There are two synthetic procedures to prepare fresnoite known from the literature: (i) crystalline powder material can be obtained by heating mixtures of $BaCO_3$, TiO_2 and SiO_2 in oxygen at 1000–1100 °C (Blasse 1968); (ii) single crystals can be obtained by heating of $2BaO:1TiO_2:2SiO_2$ and $1BaO:1TiO_2:1SiO_2$ to 1425 °C followed by slow cooling (Robbins 1970).

Our observation of the formation of fresnoite from batisite at 1000 °C is in a good agreement with the data on its synthesis and indirectly confirm its high-temperature genesis in nature. The fivefold Ti coordination in fresnoite was also discussed as an evidence of its high-temperature formation, since spectroscopic studies indicated that, in glass and recrystallized silicate melts, Ti adopts coordination numbers of four or five and may become six-coordinated upon recrystallization (Bobovich 1963; Bobovich and Petrovskii 1963). It is

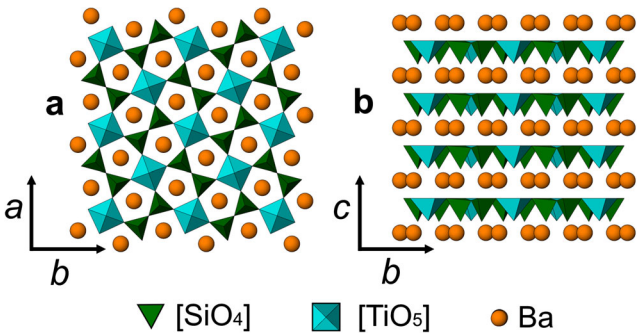

Fig. 6 Crystal structure of fresnoite projected along *c* and *a* axes (**a** and **b**, respectively)

worthy to note that fivefold Ti coordination had been observed for many other titanosiliates, e.g. lobanovite, lamprophyllite and yoshimuraite (Piilonen et al. 2003) that are certainly not high-temperature phases.

Acknowledgements We are grateful to Fernando Cámara and an anonymous referee for the detailed useful comments on the manuscript. This work was carried out using facilities of XRD and Geomodel Resource Centers of St. Petersburg State University, and supported by the Foundation of the President of the Russian Federation, grants MK-3296.2015.5 and Nsh-10005.2016.5.

References

Allen FM, Burnham CW (1992) A comprehensive structure-model for vesuvianite: symmetry variations and crystal growth. Can Mineral 30:1–18

Armbruster T, Gnos E (2000) *P4/n* and *P4nc* long-range ordering in low-temperature vesuvianites. Am Mineral 85:563–569

Belov NV (1961) Crystal chemistry of large cation silicates. Consultants Bureau, New York

Blasse C (1968) Fluorescence of compounds with fresnoite (Ba2TiSi2O8) structure. Inorg Nucl Chem 30:2283–2284

Bloembergen N, Pershan PS (1962) Light waves at the boundary of nonlinear media. Phys Rev 128:606–622

Bobovich YS (1963) Spectroscopic study of the coordination state of titanium in some glass-like substances. Optika i Spektroskopia 14: 647–654

Bobovich YS, Petrovskii GT (1963) The state of titanium in products of complete crystallization in several systems. Zhur Strukt Khim 4: 765–768

Brese NE, O'Keeffe M (1991) Bond-valence parameters for solids. Acta Crystallogr B47:192–197

Bruker (2004) Optik GmbH, Rudolf-Plank-Straße 27, D-76275 Ettlingen, Germany

Bruker AXS (2009) Topas V4.2: General profile and structure analysis software for powder diffraction data. Karlsruhe, Germany

Bruker-AXS (2014) APEX2. Version 2014.11–0. Madison, Wisconsin, USA

Chukanov NV (2014) Infrared spectra of mineral species. Springer Geochemistry/Mineralogy, London

Dolomanov OV, Bourhis LJ, Gildea RJ, Howard JAK, Puschmann H (2009) Olex2: a complete structure solution, refinement and analysis program. J Appl Crystallogr 42:339–341

Es'kova EM, Kazakova ME (1954) Shcherbakovite - a new mineral. Dokl Akad Nauk SSSR 99:837–840

Gopalakrishnan J, Ramesha K, Rangan KK, Pandey S (1999) In search of inorganic nonlinear optical materials for second harmonic generation. J Solid State Chem 148:75–80

Gorelova LA, Bubnova RS, Krivovichev SV, Krzhizhanovskaya MG, Filatov SK (2016) Thermal expansion and structural complexity of Ba silicates with tetrahedrally coordinated Si atoms. J Solid State Chem 235:76–84

Kravchenko SM, Vlasova EV, Pinevich NG (1960) Batisite — a new mineral. Dokl Akad Nauk SSSR 133:657–660

Krivovichev SV, Yakovenchuk VN, Pakhomovsky YA (2004) Topology and symmetry of titanosilicate framework in the crystal structure of shcherbakovite, $Na(K,Ba)_2(Ti,Nb)_2[Si_4O_{12}]$. Zap Vses Miner Obshchest 133(3):55–63

Kunz M, Brown ID (1994) Out-of-center distortions around octahedrally coordinated d^0-transition metals. J Solid State Chem 115:395–406

Langreiter T, Kahlenberg V (2014) TEV – a program for the determination and visualization of the thermal expansion tensor from diffraction data. Institute of Mineralogy and Petrography, University of Innsbruck, Austria

Liebau F (1982) Classification of silicates. In: Ribbe PH (ed) Orthocilicates. Rev Mineral, Mineral Soc Am 5:1–24

Liebau F (1985) Structural chemistry of silicates: Structure, bonding and classification. Springer-Verlag, Berlin

Lunkenheimer P, Krohns S, Gemander F, Schmahl WW, Loidl A (2014) Dielectric characterization of a nonlinear optical material. Sci Rep 4: 1–5

Moore PB, Louisnathan SJ (1969) The crystal structure of fresnoite, $Ba_2(TiO)Si_2O_7$. Z Kristallogr 130:438–448

Nikitin AV, Belov NV (1962) Crystal structure of batisite, $Na_2BaTi_2Si_4O_{14} = Na_2BaTi_2O_2[Si_4O_{12}]$. Dokl Akad Nauk SSSR 146:1401–1403

Piilonen PC, McDonald AM, LaLonde AE (2003) Insights into astrophyllite–group minerals. II. Crystal chemistry. Can Mineral 41:27–54

Rastsvetaeva RK, Pushcharovskii DY, Konev AA, Evsunin VG (1997) The crystal structure of K-containing batisite. Kristallografiya 42: 837–840

Robbins CR (1970) Synthesis and growth of fresnoite ($Ba_2TiSi_2O_8$) from a TiO_2 flux and its relation to the system $BaTiO_3$-SiO_2. J Res Natl Stand, Sec A 74A(2):229–232

Schmahl WW, Tillmanns E (1987) Isomorphic substitutions, straight Si-O-Si geometry, and disorder of tetrahedral tilting in batisite, (Ba, K)(K,Na)Na(Ti,Fe,Nb,Zr)Si_4O_{14}. Neu Jb Mineral, Mh 1987:107–118

Shapenkov SV, Zolotarev AA, Zhitova ES, Krivovichev SV, Krzhizhanovskaya MG (2017) High-temperature behavior of synthetic analogues of scottyite $BaCu_2Si_2O_7$ and colinowensite $BaCuSi_2O_6$. Zap Vses Miner Obshchest 146(1):115–124

Sheldrick GM (2008) A short history of SHELX. Acta Crystallogr A64: 112–116

Spek AL (2009) Structure validation in chemical crystallography. Acta Crystallogr D65:148–155

Uvarova YA, Sokolova EV, Hawthorne FC, Liferovich RP, Mitchell RH (2003) The crystal chemistry of shcherbakovite from the Khibina massif, kola peninsula, Russia. Can Mineral 41:1193–1201

Uvarova YA, Sokolova EV, Hawthorne FC, Liferovich RP, Mitchell RH, Pekov IV, Zadov AE (2010) Noonkanbahite, $BaKNaTi_2(Si_4O_{12})O_2$, a new mineral species: description and crystal structure. Mineral Mag 74:441–450

Viani A, Palermo A, Zanardi S, Demitri N, Petrı'cek V, Varini F, Belluso E, Ståhl K, Gualtieri AF (2015) Structure and stability of $BaTiSi_2O_7$. Acta Cryst B71:1–11

Williams DJ (1984) Organic polymeric and non-polymeric materials with large optical nonlinearities. Angew Chem Int Ed Engl 23:690–703